Virology 529 (2019) 152–159

Contents lists available at ScienceDirect

Virology

journal homepage: www.elsevier.com/locate/virology

Identification of the Epstein Barr Virus portal

Robert J. Visalli*, Adam M. Schwartz, Shivam Patel, Melissa A. Visalli

Department of Biomedical Sciences, Mercer University School of Medicine, Savannah, GA 31404, USA

ARTICLE INFO

Keywords:
Portal
Virus structure
Herpesvirus
Epstein Barr Virus
EBV

ABSTRACT

Little is known about Epstein Barr Virus (EBV) proteins that participate in viral DNA cleavage and packaging. Genes encoding potential terminase subunit and portal protein homologs include BGRF1/BDRF1, BALF3, BFRF1A and BBRF1 respectively. EBV mutants with deletions in one or more of these genes were impaired for DNA packaging (Pavlova et al., 2013). In the current study, BBRF1 oligomers were purified from recombinant baculovirus infected insect cell extracts. Transmission electron microscopy revealed that purified EBV portals retained features typically found in other portals including a central channel with clip, stem and wing/crown domains. Although compounds have been identified that target DNA encapsidation in human cytomegalovirus, herpes simplex viruses and varicella-zoster virus, the identification of new EBV targets has lagged significantly. Characterization of the EBV portal will direct studies aimed at developing potential small molecular inhibitors of the EBV encapsidation process.

1. Introduction

Epstein-Barr Virus (EBV) is a geographically ubiquitous human gamma-1 herpesvirus that primarily infects B-cells and epithelial cells (Münz, 2015). As with the other human herpesviruses, EBV has both lytic and latent stages. The lytic state allows the production of infectious virions capable of infecting new cells. The latent state establishes life-long persistent infection in memory B lymphocytes with limited viral gene expression thus escaping immune clearance (Münz, 2015). By adulthood more than 95% of humans harbor latent EBV (Houldcroft and Kellam, 2015).

EBV infection is common in children and easily spread through contact with saliva. Most infections are asymptomatic, however primary infections result in a significant number of cases of infectious mononucleosis (IM) (Münz, 2015). EBV is estimated to cause approximately 125,000 new cases of IM in the US each year which translates to more than 3 million cases worldwide (Cohen et al., 2011). Improved living conditions have resulted in a shift in IM epidemiology until adolescence or later. IM typically presents as fever, sore throat, swollen lymph nodes and for some individuals, fatigue lasting several months (Turner and Taylor, 2013). In a 2015 review "Infectious Mononucleosis", Balfour et al. (2015) noted that a major goal for EBV researchers is to "to discover specific anti-EBV drugs to treat infectious mononucleosis" and that "the field of anti-cytomegalovirus drug development is much further along than that of EBV." To date, there are no clinically proven treatments for IM.

The association of EBV with gastric carcinoma, nasopharyngeal carcinoma, and Hodgkin's and Burkitt's lymphomas contribute to ~1% of all cancer cases worldwide (Klein et al., 2007). Immunosuppressed individuals are at risk for EBV-induced immunoblastic proliferations (George et al., 2012; Klein et al., 2007). The National Institutes of Health estimates that nearly 200,000 cases of cancer per year (worldwide) can be attributed to EBV (Cohen et al., 2011; Turner and Taylor, 2013). There are a number of novel therapies under study for EBV–associated malignancies. These include (i) adoptive T-cell therapy (e.g. donor lymphocyte infusions) (Eiz-Vesper et al., 2012; McLaughlin et al., 2018), (ii) inhibitors of EBV activated signaling pathways (Akt inhibitors, Rapamycin) (Chen, 2012; Kosowicz et al., 2017), (iii) proteasome inhibitors (Hui et al., 2017), (iv) recombinant vaccines (to prevent primary infection or target nasopharyngeal carcinoma) (Cui et al., 2016; Lin et al., 2017; Rajcani et al., 2014), and (v) lytic induction combined with anti-herpesviral drugs (ganciclovir/valganciclovir) (Feng et al., 2004; Lee et al., 2015; Stoker et al., 2015).

Understanding the function(s) of lytic cycle proteins may reveal novel targets for antiviral chemotherapy of EBV associated diseases. Numerous studies have documented the expression and role of EBV latency proteins in B-cell transformation. Not surprisingly, the study of EBV latency as it relates to EBV-associated malignancies has predominated over lytic cycle research. However, evidence suggests that the EBV lytic cycle likely contributes significantly to EBV pathogenesis (Dolcetti et al., 2013). Lytically infected cells and or proteins can be detected in EBV-associated tumors (Hu et al., 2016; Li et al., 2016; Yu

* Correspondence to: Department of Biomedical Sciences, 1250 E. 66th St., Savannah, GA 31404, USA.
E-mail address: visalli_rj@mercer.edu (R.J. Visalli).

https://doi.org/10.1016/j.virol.2019.01.003
Received 4 September 2018; Received in revised form 21 December 2018; Accepted 3 January 2019
Available online 10 January 2019

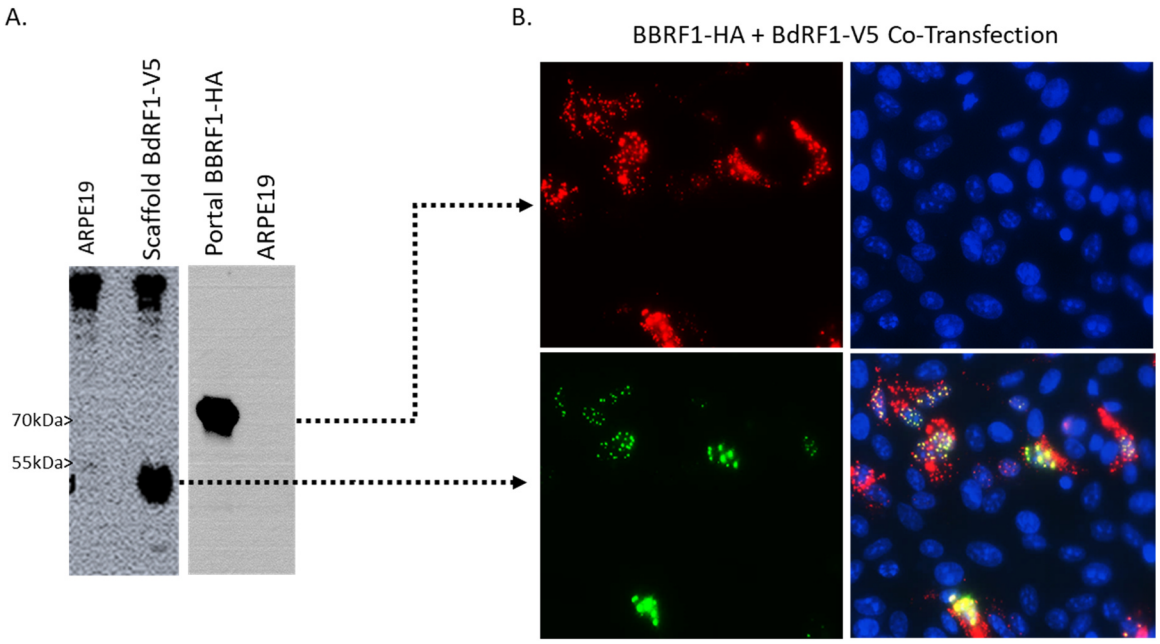

Fig. 1. Expression and co-localization of the EBV portal and scaffold proteins. (A) Immunoblot analysis was performed with anti-V5 or anti-HA primary antibody on mock and pcDNA3.1D/V5-BdRF1 or mock and pcDNA3.1D/HA-BBRF1 transfected ARPE19 cell extracts. (B) Immunofluorescence analysis of APRE19 cells co-transfected with BBRF1-HA and BdRF1-V5. Cells were fixed at 24 h post-transfection, stained with DAPI, and incubated with MAB-anti V5 DyLight-488 and MAB-anti HA DyLight-550 conjugates. BBRF1 expressing cells appear red, BdRF1 expressing cells are green and cell nuclei stained with DAPI are blue.

et al., 2018). New infectious virus might spread locally and systemically, infecting new B cells and increasing the pool of latently infected cells. Furthermore, several studies have reported that prophylactic treatment of transplant patients with antivirals (targeting lytically replicating EBV) decreased EBV-associated lymphoproliferative disease (Tse and Kwong, 2015). A number of studies have suggested combining antivirals with lytic cycle inducers capable of triggering EBV lytic replication (Giunco et al., 2015; Kanakry and Ambinder, 2013; Wildeman et al., 2012). *In vivo*, EBV strains defective for lytic replication are less effective in inducing EBV-positive lymphoproliferations in SCID mice (Hong et al., 2005). In a humanized mouse model (NOD/LtSz-scid/IL2Rγnull) animals infected with EBV have increased numbers of tumors compared to lytic cycle-defective EBV (Ma et al., 2011). EBV lytic replication plays a crucial lymphomagenic role and targeting the lytic cycle may be an effective way to reduce not only infectious mononucleosis but EBV-associated cancers. None of the available herpesviral DNA replication inhibitors (nucleoside, nucleotide, and pyrophosphate analogs) have been approved for treatment of EBV diseases (Gershburg and Pagano, 2005). Hence, understanding both the latent and lytic cycles is critical to the development of new therapeutic strategies that target gammaherpesvirus-associated diseases (EBV and perhaps KSHV neoplasias) (Jha et al., 2016). Antiviral compounds with novel mechanisms of action may prove to be useful clinically, and there is room for improvement over current options with respect to side effects profiles, bioavailability and efficacy against potential antiviral drug-resistant EBV (Gershburg and Pagano, 2005; Topalis et al., 2018; Walling et al., 2003).

During the replication of all herpesviruses, newly synthesized viral DNA is cleaved into unit length genomes, and packaged into pre-formed empty viral capsids by a virus encoded molecular motor that includes the viral terminase and portal proteins (Mettenleiter et al., 2006; Visalli and van Zeijl, 2003). This motor has been well described for the dsDNA bacteriophages (Allemand et al., 2012; Oliveira et al., 2013) but less so for herpesviruses. Comparatively speaking, there are only a few studies describing the EBV lytic proteins that participate in viral genome cleavage and packaging. Small molecule compounds have been described that target the HSV and VZV portal proteins (van Zeijl et al., 2000; Visalli et al., 2003; Visalli and van Zeijl, 2003; Yasui et al., 2017). Our laboratory is interested in expanding encapsidation research to include the gammaherpesviruses in an effort to identify EBV and HHV-8 portal protein inhibitors.

Previously the portal of the human gamma-2 herpesvirus, human herpesvirus 8 (HHV-8), was characterized via cryoelectron tomography. The portal monomer, putatively encoded by pORF43, forms an oligomeric complex at a single capsid vertex. Studies by Deng et al. localized the portal internally, below the floor of the major capsid protein (Deng et al., 2007; Russo et al., 1996). To date, the HHV-8 portal oligomer has not been isolated or characterized. Here, we propose that BBRF1 encodes the EBV portal protein. The EBV portal has not been isolated and characterized, nor identified in EBV nucleocapsids. However, BBRF1 mutant viruses do not package viral DNA, implicating BBRF1 in the encapsidation process (Pavlova et al., 2013). Based on the BBRF1 mutant virus phenotype, homology modeling to phage and other herpesvirus portal proteins, and the results presented in this study, we show that BBRF1 encodes the EBV portal protein monomer. The lack of approved drugs for treating EBV diseases merits studies focused on the identification and characterization of viral DNA encapsidation proteins as potential antiviral targets.

2. Results

2.1. Expression and co-localization of the EBV BBRF1 and BdRF1 proteins

Sequence analysis suggested that the BBRF1 and BdRF1 genes encode the EBV portal and scaffold proteins respectively (Baer et al., 1984; Visalli and van Zeijl, 2003). Protein-protein interactions between herpesvirus scaffold and portal proteins were reported previously for herpes simplex virus type 1 (HSV-1). Portal-scaffold complexes have been co-immunoprecipitated from transfected or virus infected cell extracts, and shown to co-localize in the nucleus, the site of herpesvirus DNA encapsidation (White et al., 2003; Yang and Baines, 2008).

To determine if portal-scaffold interactions were conserved for EBV, the BBRF1 and BdRF1 open reading frames were cloned into a mammalian expression vector containing either a HA (pcDNA3.1D/HA-BBRF1) or V5 (pcDNA3.1D/V5-BdRF1) C-terminal epitope tag. Western blotting of transfected cell extracts confirmed the expression of BBRF1-

HA (73 kDa) and BdRF1-V5 (42 kDa) (Fig. 1A). The sizes were consistent with the predicted molecular weights of BBRF1 (68.5 kDa) and BdRF1 (36.1 kDa) plus either the HA or V5 (~5 kDa) epitope tag. Immunofluorescence analysis of BBRF1-HA and BdRF1-V5 expressed in transiently transfected ARPE19 cells showed that BBRF1 localized to the cytoplasm whereas BdRF1 localized exclusively to the nucleus (Fig. 1B). These results were consistent with those reported for expression of BBRF1 and BdRF1 in Cos-7 cells (Cai et al., 2017). However, BdRF1 showed punctate nuclear staining in ARPE19 cells as opposed to the pan-nuclear staining observed in Cos-7. BBRF1 showed speckled cytoplasmic staining similar to that reported after expression in Cos-7 cells. Co-transfection of pcDNA3.1D/HA-BBRF1 and pcDNA3.1D/V5-BdRF1 into ARPE19 cells showed that some BBRF1 co-localized with BdRF1 in the nucleus (Fig. 1B), the site of herpesvirus DNA encapsidation. Nuclear translocation of BBRF1 required expression of BdFR1. This is in contrast to the HSV-1 portal protein, pUL6, which localizes to the nucleus without the aid of additional viral proteins (White et al., 2003).

2.2. Recombinant baculovirus expression of the BBRF1 gene encoding the putative EBV portal protein monomer

Although BBRF1 had not been show to encode the portal, previous studies showed that deletion of BBRF1 resulted in the accumulation of empty capsids in mutant infected cells (Pavlova et al., 2013). The presence of only empty capsids is consistent with a role for BBRF1 in viral DNA encapsidation. Therefore, PCR primers were designed based on the EBV 98-5 strain BBRF1 gene and used to produce a 1842 bp amplicon consistent with the predicted size of the full length BBRF1 open reading frame. This product was cloned into the pFastBac NT-TOPO vector using the Bac-to-Bac N-His TOPO Cloning Kit and resulted in the addition of a N-terminal 6xHis epitope tag. This construct was used to generate bacmid Bac-BBRF1-6xHis. Bac-BBRF1-6xHis and control Bac-GUS DNAs were isolated and transfected into Sf9 insect cell cultures. Cultures showing cytopathic effect were expanded to prepare recombinant baculovirus stocks. High titer stocks of Bac-BBRF1-6xHis and Bac-GUS were used to infect Sf9 cells to prepare infected cells extracts for western blot and silver stain analyses. Western blotting with an anti-His antibody detected a protein of 71 kDa (Fig. 2B). The size was consistent with the predicted molecular weight of BBRF1 (68.5 kDa) and plus the N-terminal 6xHis epitope tag (~2.5 kDa). No proteins were detected in Bac-GUS infected sf9 control extracts. Silver staining revealed a protein of approximately the same molecular weight as that observed in the western blot (Fig. 2A) for Bac-BBRF1-6xHis infected sf9 cells but was absent in Bac-GUS control extracts.

2.3. Gradient fractionation of Bac-BBRF1 infected Sf9 cell extracts

Oligomeric herpesvirus portal proteins have been purified from Sf9 extracts fractionated via sucrose density gradient centrifugation (Dittmer and Bogner, 2005; Holzenburg et al., 2009; Howard et al., 2012; Newcomb et al., 2001; Visalli and Howard, 2014). Baculovirus infected sf9 cells were processed in the presence of 1 M arginine to enhance solubility of potential BBRF1 oligomers. Gradient fraction samples were not directly suitable for analysis due to the high concentrations of arginine. Therefore, proteins in each fraction were precipitated prior to SDS-PAGE. Western analysis showed a 71 kDa protein in gradient fractions 4 and 12–14 (Fig. 2D). No proteins were detected in the Bac-GUS control samples blotted with the anti-His antibody (Fig. 2C). Fraction 4, near the top of the gradient, was selected for analysis by negative staining and transmission electron microscopy. Although positive for the 71 kDa portal protein, fractions toward the bottom of the gradient (fraction 14) contained large aggregates unsuitable for imaging.

2.4. Transmission electron microscopy of gradient purified BBRF1-6xHis

Aliquots taken from fraction 4 were prepared for TEM analysis. Individual portal oligomers with axial and non-axial perspectives were observed Fig. 3A. The central channel was clearly visible in several portals in Fig. 3B. A diameter of ~15–20 nm was consistent with that reported for the HHV-8 portal (Deng et al., 2007). Fig. 3C was a low magnification image of a sample of concentrated portal oligomers. Figs. 3D and 3E show an example of one portal oligomer captured at an approximately 45° angle with respect to the grid surface. The portal showed the typical mushroom appearance with the portal crown at the wider portion of the image while the stem and clip regions resided at the narrow end.

2.5. Oligomeric state of in vitro purified BBRF1-6xHis

During capsid assembly, phage and herpesvirus portals are found to obtain 12-fold symmetry at a single capsid vertex. *In vitro* expression and purification of bacteriophage and herpesvirus portal proteins can yield a range of oligomeric structures including un-, do-, and tri- decamers. The oligomeric nature of the EBV portal described in this study was examined by native gel protein electrophoresis and western blotting. A sample of the same Bac-BBRF1-6xHis gradient fraction characterized by electron microscopy was solubilized in 1% DDM, separated via native page and transferred to membranes for western blotting with THE HIS antibody. A corresponding gradient fraction of Gus-BAC sample was run in parallel as a negative control. Analysis revealed a

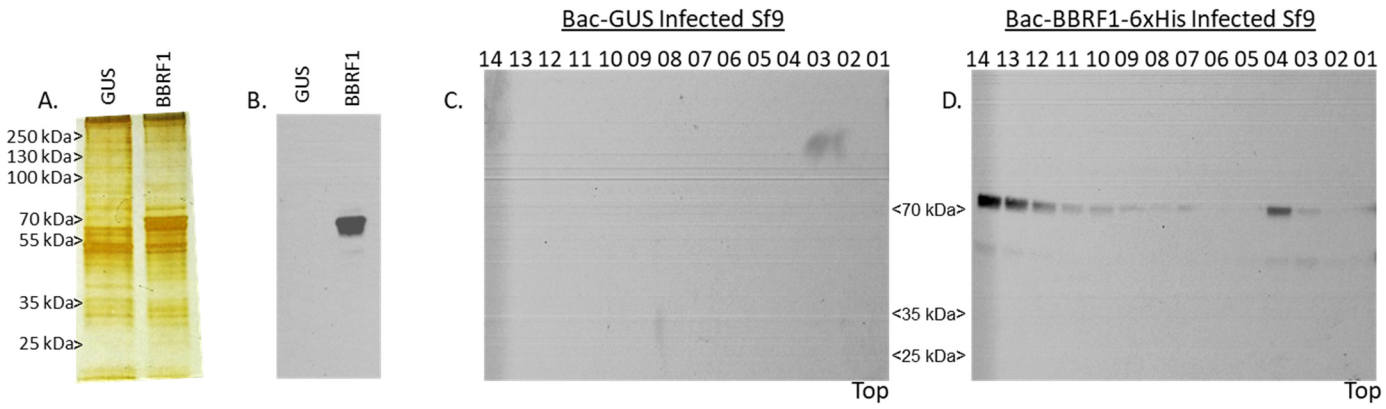

Fig. 2. Detection of BBRF1-6xHis in recombinant baculovirus infected Sf9 cells. Sf9 insect cell cultures were infected with Bac-GUS (negative control virus) or Bac-BBRF1-6xHis viruses. The presence of BBRF1-6xHis in infected cell extracts was observed by (A) silver staining or (B) immunoblotting with anti-His antibody. Sucrose gradient fractionation of Bac-GUS or Bac-BBRF1-6xHis processed, Sf9 infected insect cell extracts. Fourteen gradient fractions were analyzed for the presence of the 71 kDa BBRF1-6XHis protein. (D) The strongest BBRF1 signal was detected in fractions 4 and 12–14. (C) No proteins were detected in the Bac-GUS control samples.

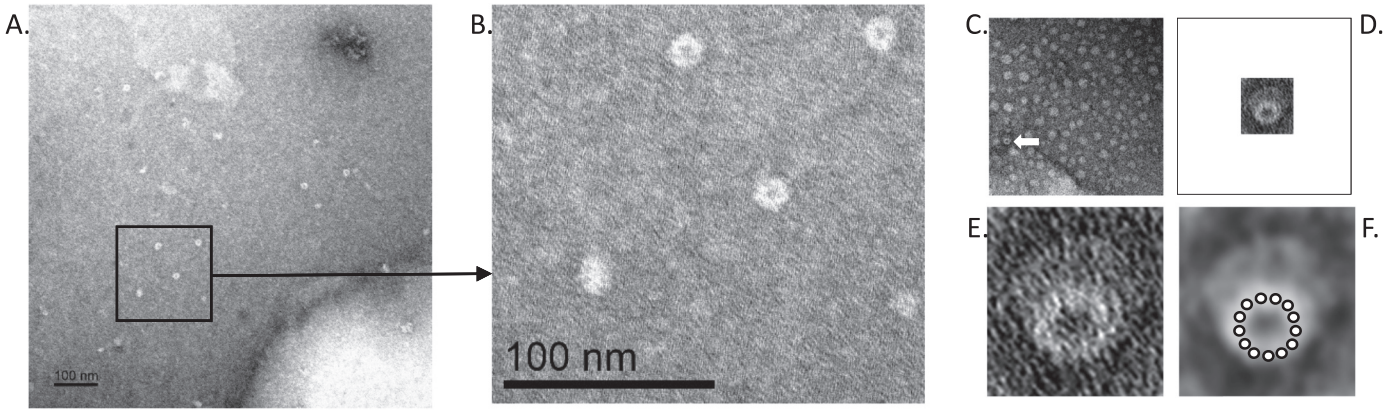

Fig. 3. Transmission electron microscopy of Bac-BBRF1-6xHis sucrose gradient fraction #4. Samples applied to copper grids were stained with 1% uranyl acetate and imaged using a JEOL 2100 Plus TEM fitted with a Gatan 4K × 4K Pixel OneView CMOS CCD camera. Panel A: low magnification image of diluted sample; Panel B enlarged section of a portion of the image in Panel A; Panel C: low magnification image of undiluted sample; Panel D: enlarged image of a portal from Panel C (white arrow); Panel E: enlarged and contrast enhanced image from Panel D; and Panel F: estimated distribution of 13 monomeric clip regions at the narrow end of the portal oligomer shown in Panels D and E.

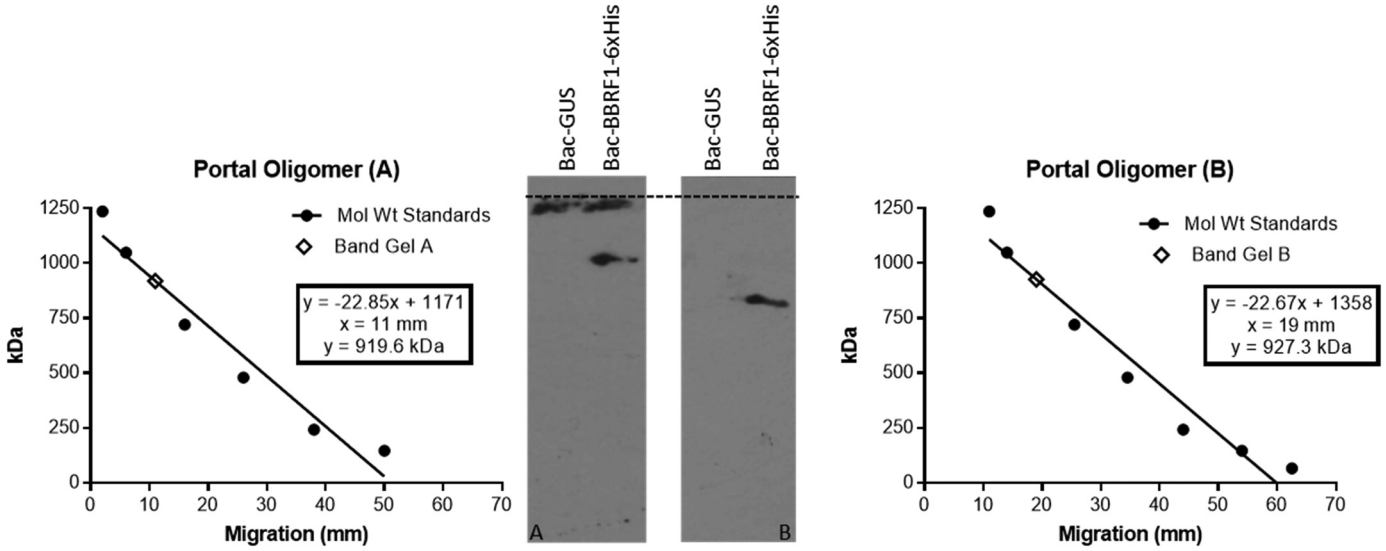

Fig. 4. Estimating the oligomeric nature of the EBV portal by blue native gel electrophoresis and western blotting. Aliquots from Bac-GUS or Bac-BBRF1-6xHis gradient sample #4 were processed as described in the materials and methods, loaded on 3–12% Bis-Tris NativePAGE gels and separated by electrophoresis. The paired samples were processed and analyzed in two separate experiments. Immunoblotting was performed using THE HIS primary antibody and secondary goat anti mouse-HRP conjugated antibody. NativeMark unstained protein markers were cut from the gel prior to blotting. Stained protein marker migration was measured from the top of each gel and plotted. A best fit line was generated for experiment A and B and portal size was estimated using the polynomial equation generated for each set of standards and migration of single band observed in each experiment. Assuming a molecular weight of ~70.9 kDa for BBRF1-6xHis, experiment A and B predict portal oligomers of approximately 13.0 and 13.1 respectively.

single prominent band with an estimated molecular weight of 920 or 927 kDa from two independent experiments (Fig. 4). Using the estimated EBV portal monomer size of 70.9 kDa (including the His tag), the oligomeric state of in vitro purified EBV portal was determined to be a 13-mer. Fig. 3F depicts how 13 clip regions might be spaced at the narrow end of a tridecamer. This is consistent with previous reports that in vitro expressed portals for some viruses may have a significant population of tridecamers. For example, in vitro purified *Bacillus subtilis* SPP1 phage connector (gp6 portal) was once thought to be a tridecamer that represented a naïve assembly form with low affinity for viral DNA and/or DNA packaging machinery. It was speculated that upon incorporation into the capsid, conversion to a dodecamer locked the portal into the capsid vertex (Lurz et al., 2001). The tridecamer form of the SPP1 portal is now thought to be an artifact of the in vitro purification process (Lorenzen et al., 2008). Although we cannot rule out that the EBV portal exists as a tridecamer in EBV capsids, we speculate that consistent with other phage and herpesvirus portals, a portal with 12-fold symmetry will represent the functional version found in EBV virions.

2.6. Modeling the BBRF1 monomer

To date, there are no crystal structure or tomography data for any herpesvirus portal. Recently, the HSV-1 portal-vertex was reconstructed showing the protein-protein interactions found at the portal specific capsid vertex, but the portal itself (U_L6) could not be characterized in similar detail (McElwee et al., 2018). Although density corresponding to the HSV-1 portal could be observed just inside the capsid shell, the data was insufficient to reconstruct the portal oligomer lying below the vertex. Therefore, we employed a bioinformatics approach to generate a predicted ribbon structure for the EBV portal protein monomer. Structural homology to ds DNA phage portals was used to model the EBV portal including the fact that all portals appear to contain a conserved portal core or stem region (Kornfeind and Visalli, 2018). A likely

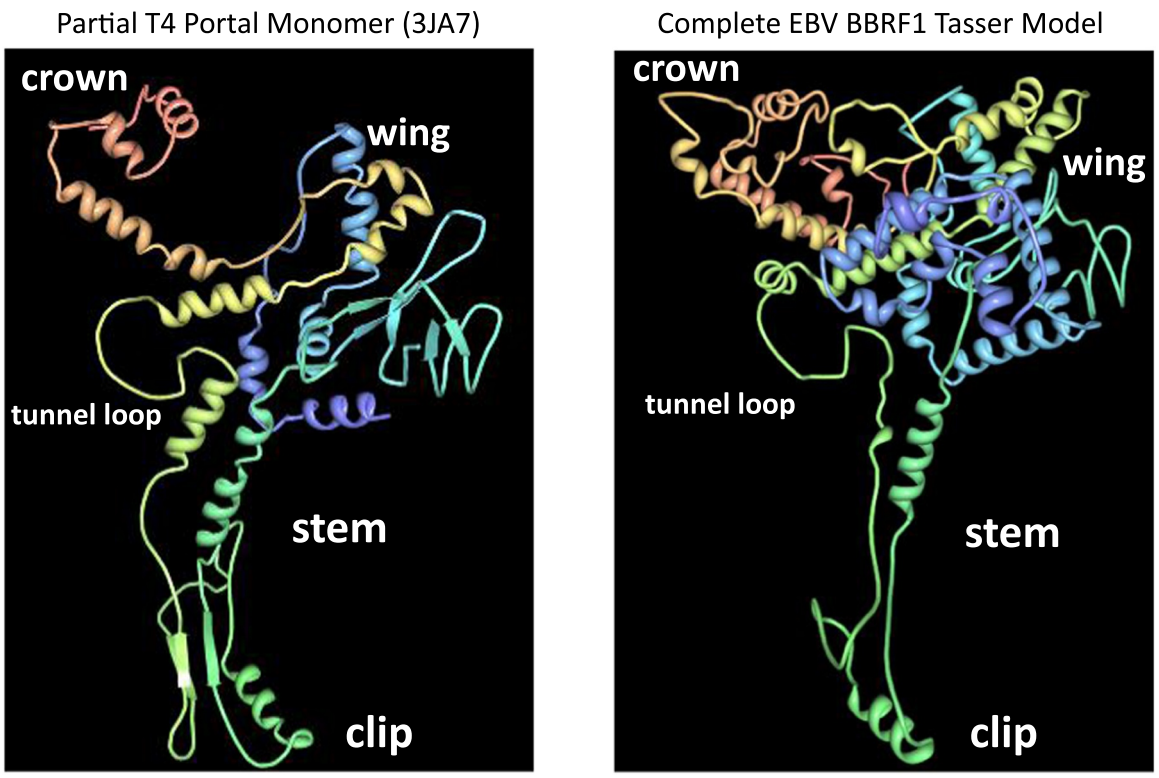

Fig. 5. Tasser model for the EBV portal monomer encoded by BBRF1. The full length 613 amino acid BBRF1 sequence was submitted to the Tasser server for structural modeling. The T4 phage portal monomer is provided for comparison (PDB 3JA7). The key structural features are labeled for each protein. Monomers assemble into oligomers to form complete portals. The clip regions are predicted to point toward the outside of the virus particle and in bacteriophage have been shown to bind the terminase subunits during DNA encapsidation. The tunnel loop forms the interior where the DNA passes through a narrow channel of the oligomeric portal.

structure for the EBV portal monomer was derived based on predicted secondary structure of the BBRF1 amino acid sequence combined with known structural data for bacteriophage portals from the PDB database (e.g. T4: 3JA7, P22: 5JJ3, SPP1: 2JES, Phi-29: IH5W). Submitting this information to the online I-TASSER server resulted in the generation of the most likely EBV monomer structures. Fig. 5 shows the EBV portal ribbon structure that most closely resembled those of known bacteriophage portals. The predicted model displays key conserved structural features of portals including the stem containing the α-3 helix in the stem, the putative terminase binding clip region, the unstructured tunnel loop that contacts the DNA, and domains making up the crown and wing regions. The biggest difference compared to phage portals is a poorly defined α-5 stem helix. This model represents the most accurate estimation of a herpesvirus portal monomer to date.

3. Discussion

This is the first report describing the cloning and expression of BBRF1, confirmed here to form the EBV capsid portal. A 71 kDa N-terminal 6xHis tagged BBRF1 monomer was the major product detected in recombinant baculovirus infected Sf9 cell extracts. Tagging the N-terminus of BBRF1 did not prevent the assembly of EBV portals, however, it is not known if the portals are functional. The EBV portal appeared relatively homogenous in TEM experiments and should provide an excellent substrate for further structural studies.

Previous work with the VZV portal was more difficult, including excessive aggregation and variability in the observed portal products (Howard et al., 2012). Perhaps the properties and smaller molecular mass of the EBV monomer compared to the VZV monomer (pORF54 = ~87 kDa) (Kornfeind and Visalli, 2018) result in more efficient and consistent oligomerization. This is consistent with the single protein band observed during native PAGE analysis that suggested that purified EBV portals were almost exclusively tridecamers.

Information on the assembly and structure of the EBV portal has both fundamental and translational relevance, and is a potential target for antiviral drug development. There are no approved drugs for the treatment of any EBV disease. Several drugs including nucleoside analogs did not prove consistently effective when tested in clinical trials involving infectious mononucleosis and EBV related cancer. Study of EBV portal and potential EBV encapsidation inhibitors is strategic for several reasons including (i) there is little information on the EBV proteins that participate in viral DNA encapsidation and (ii) there are no approved drugs to treat EBV diseases including infectious mononucleosis and an increasing number of EBV-associated cancers.

4. Materials and methods

4.1. Cell culture

ARPE19 cells (human retinal pigmented epithelial cells; ATCC CRL-2302) were maintained at 37 °C and 5% CO_2 in minimal essential medium (MEM) supplemented with 5% fetal bovine serum (FBS), 2 mM L-glutamine, 100 U/ml penicillin, 100 μg/ml streptomycin, and 0.25 μg/ml amphotericin B. Sf9 insect cells (EMD Millipore Novagen) were cultured in SFX-Insect cell serum free media (HyClone) at 27 °C in shaker flasks.

4.2. Immunofluorescent microscopy

Cells seeded on coverslips were incubated overnight and then transfected or co-transfected with 1.5 μg of plasmid DNA using Lipofectamine LTX (Life Technologies). After 24 h coverslips were washed twice in phosphate-buffered saline (PBS) and fixed in 1:1 MeOH:Acetone for 20 min at −20 °C. Coverslips were washed twice in

PBS and incubated with 5% skim milk overnight at 4 °C. Coverslips were washed twice in 3% BSA/PBS and incubated at room temperature (RT) for 1 h with antibody diluted in 3% BSA /PBS. Antibodies included MAB-anti V5 DyLight-488 or MAB-anti HA DyLight-550 conjugates (Thermo Fisher Scientific). Coverslips were washed five times for 5 min each with 3% BSA /PBS and stained with 1 μg/ml Hoechst for 15 min. Coverslips were mounted with DAPI fluoromount-G (Southern Biotech) and observed using a Nikon Eclipse T*i* fluorescent microscope. Images were captured at 20 x or 40 x and analyzed using NIS-Elements (Nikon).

4.3. Cloning EBV BBRF1

Template DNA was isolated from B98-5 infected HEK cells. Cells were washed twice in ice-cold PBS and lysed with 800 ul of TES (10 mM Tris, 0.6% SDS, 10 mM EDTA, 50 mM NaCl) plus 20 μg RNase A. Cell monolayers were mechanically dislodged and placed into a microfuge tube. The lysate was incubated at 37 °C for 30 min then proteinase K was added and the mixture incubated overnight at 37 °C. The lysate was then extracted with an equal volume of phenol, 1:1 phenol:chloroform and finally chloroform. DNA was precipitated by adding 200 ul of 4 M NaCl and two volumes of 100% EtOH. DNA was collected by centrifuging for 5 min at 16,000 × *g*. Pelleted DNA was washed with 70% EtOH, briefly dried and resuspended in 200 ul of 10 mM Tris pH 8.5. Extracted DNA served as a template to generate BBRF1 (1839 bp) or BdRF1 (1035 bp) DNA amplicons using primer sets BBRF1F-CACCATGTTCAA CATGAACGTGGAC/R- ACTTCCAGCACCAGGCGG or BdRF1 F- CACCATGCTATCAGGTAACGCAGG/R- AGCCACGCGTTTATTCA GCA. Amplicons were cloned into pcDNA3.1D/V5-HIS-TOPO (Invitrogen) and confirmed by DNA sequence analysis (Eurofins Genomics). To replace the V5 tag with a HA epitope tag, a BBRF1 amplicon was generated using a modified reverse primer R-CTAAGCG TAATCTGGAACATCGTATGGGTA ACTTCCAGCACCAGGCGG. All PCR reactions were performed using Phusion DNA polymerase (Thermo Fisher Scientific).

The Bac-to-Bac N-HIS Expression System (Invitrogen) was used to create a recombinant baculovirus containing the EBV BBRF1 gene. BBRF1 primer set BBRF1FBac- ATGTTCAACATGAACGTGGAC/RBac-TTAACTTCCAGCACCAGGCG was used to generate a full length1842 bp BBRF1 product that was subsequently cloned into the pFastBac/NT-HIS vector.

4.4. Generating BBRF1 recombinant baculovirus

DH10Bac *E. coli* were transformed to generate recombinant baculovirus Bac-pBBRF1-6xHis according to the manufacturer's instructions (Bac-to-Bac, Invitrogen). A control Bac-GUS with a β-glucuronidase reporter gene was also constructed using the system. Sf9 insect cells (5×10^5) were transfected with Bac-pBBRF1 or Bac-GUS DNA complexed with Cellfectin II Reagent (Invitrogen) in SFX media (Hyclone). Sf9 cultures were observed for cytopathic effect and culture supernatants containing recombinant baculoviruses were harvest and stored in the dark at 4 °C.

4.5. Expression of pBBRF1-HA and BdRF1-V5 in ARPE19 cells

Plasmids (1.5 μg) encoding C-terminal epitope tagged EBV proteins were transfected into to ARPE19 cells using Lipofectamine LTX (Life Technologies). Transfected cells were collected by centrifugation at 1500 rpm for 10 min at 4 °C. Cell pellets were lysed by resuspending in EZ buffer (100 mM Tris pH 7.4, 100 mM KCl, 1% NP40, 10 uM ZnOAc, 10% glycerol) containing protease inhibitors and incubating on ice for 10 min. The cell lysates were centrifuged at 16,000 × *g* and the resulting pellets were solubilized in 2 x Laemmli buffer with β-mercaptoethanol. Samples were heated at 98 °C for 8 min, separated on a 10% Tris-glycine acrylamide gel (BioRad), transferred to PVDF membrane and incubated with either anti-V5 or anti-HA primary antibody (Genscript) followed by a HRP conjugated anti-mouse secondary antibody. Clarity Western ECL Substrate (BioRad) was used to perform chemiluminescent detection.

4.6. Expression of BBRF1-6xHis in Sf9 cells

Sf9 cell cultures were infected at a ~MOI of 1 for 48 h with recombinant baculovirus Bac-BBRF1-6xHis stock. Infected cells were collected by centrifugation at 4000 rpm for 10 min at 4 °C. Cell pellets were processed as described above except that membranes were incubated with THE HIS primary antibody (Genscript). Samples were also processed for silver staining stained using the Pierce Silver Stain Kit (Thermo Fisher Scientific).

4.7. Extraction and gradient fractionation of pBBRF1-6xHis from Sf9 cells

Sf9 insect cell cultures infected with Bac-BBRF1-6xHis or a Bac-GUS negative control viruses were incubated with shaking at 27 °C for 48 h. All purification steps were performed at 4 °C unless otherwise indicated. Cells were harvested at 4500 rpm for 5 min at RT ~1.0 ml of packed cells were washed with phosphate buffered saline (PBS, pH 7.4) containing protease inhibitors, pelleted at 4500 rpm for 5 min at RT, and resuspended in 4 ml of PBS with protease inhibitors. Cells were lysed by three cycles of freezing and thawing at −196 °C (liquid nitrogen)/37 °C. The lysate was centrifuged for 5 min at 16,000 × *g*and the supernatant discarded. The pellet was resuspended in 1.0 ml of TNE (pH 8.0) containing 2% Triton X-100, 10 mM dithiothreitol and protease inhibitors, briefly sonicated with a micro-tip probe and incubated for 30 min on ice. The suspension was centrifuged at 16,000 × *g* for 5 min at RT and the supernatant discarded. The pellet was resuspended in 1.0 ml of TNE containing 20 mM $MgSO_4$, 0.5 mg/ml of DNase I and protease inhibitors followed by a 10 min incubation at RT on a rocker-rotator. The suspension was centrifuged at 16,000 × *g* for 5 min and the supernatant discarded. The pellet was resuspended in 2.0 ml of 20 mM Tris pH 7.4 containing 1 M arginine and incubated for 10 min on a rocker-rotator. The resulting solution was clarified by centrifugation at 32,000 × *g* for 30 min at 4 °C. The supernatant was applied to the top of a 10–55% sucrose gradient prepared in 20 mM Tris-HCl pH 7.4 containing 1 M arginine. The gradients were centrifuged overnight at 23.4 K rpm at 4 °C in a SW-41 Ti rotor (Beckman). Gradients were fractioned into approximately 0.5 ml aliquots from top to bottom using a gradient fractionator (Labconco).

4.8. Precipitation of pBBRF1 from gradient samples and analysis via western blotting

Sucrose gradient fractions were precipitated to remove sucrose by mixing with four volumes of MeOH, an equal volume of chloroform and three volumes water. Mixtures were vortexed followed by brief centrifugation at 1000 rpm between each addition. The aqueous top layer was removed carefully to avoid disturbing the proteinaceous interface. Three volumes of MeOH was added and samples were centrifuged at 16,000 × *g* for 5 min to pellet proteins. Samples were air dried and processed for western blotting with THE HIS antibody as described above.

4.9. Transmission electron microscopy of portal-containing gradient samples

Gradient fractions likely to contain portals were applied to copper grids for 30 s, washed twice with 10 mM Tris pH 7.4, and stained with 1% uranyl acetate. Grids were imaged using a Jeol 2100 Plus 200 kV TEM.

4.10. Native gel PAGE and western blotting of purified portals

The molecular mass of purified Bac-BBRF1-6xHis portal observed in gradient fraction 4 was determined by blue native polyacrylamide gel electrophoresis and western blotting (Motwani et al., 2017). The corresponding gradient fraction from Gus-BAC infected SF9 cells was included as a control. Proteins were precipitated from a 50 ul sample of fraction 4 for Bac-BBRF1-6xHis or Gus-BAC. Protein pellets were solubilized by adding 20 ul of 20 mM Tris pH 7.4, 100 mM NaCl and 1% DDM (n-Dodecyl β-D-maltoside) and incubated at room temperature for 30 min with gentle resuspension. 2.5 ul of solubilized portal was added to 2.5 ul 2 x NativePAGE sample buffer and 5 ul water. Samples were loaded onto a 3–12% NativePAGE Bis-Tris gel (Thermo Fisher Scientific). Proteins were separated by electrophoresis in dark cathode buffer at 150 V constant voltage at 4 °C. After 1 h the dark cathode buffer was changed to light cathode buffer and electrophoresed for an additional 90 min at 150 V/4 °C. Immunoblotting was performed using THE HIS primary antibody (Genscript) and secondary goat anti-mouse HRP conjugated antibody (Invitrogen). NativeMark unstained protein marker (Thermo Fisher Scientific) was run in parallel with the samples and cut from the gel prior to transfer, stained with 0.25% Coomassie blue in 10% acetic acid/45% MeOH overnight and destained in 10% acetic acid/45% MeOH. Stained protein marker migration was measured from the bottom of the well. Portal size was estimated by comparing migration of the protein found in the sample lanes to the NativeMark protein standards. Simple linear regression (Prism GraphPad) was used to generate a best fit line and a corresponding first-order polynomial equation to estimate the molecular mass of the portal oligomer observed on each blot.

4.11. Modeling pBBRF1

I-TASSER Protein Structure and Function Prediction (Iterative Threading Assembly Refinement) is a protein structure and function prediction program (Yang et al., 2015). User-identified structural templates selected from the Protein Data Base (PDB) were used to construct full-length atomic models by iterative template fragment assembly simulations. Target function was predicted by threading the 3D model through a protein function database. Protein Workshop (Berman et al., 2000) is available via the PDB site to visualize 3D protein structures (monomers or complexes) in high-quality ribbon style

Acknowledgments

EBV infected cell pellets for DNA extraction were kindly provided by Dr. Gretchen Bentz, Mercer University School of Medicine, Macon, GA.

Author contributions

R.V. and M.V. conceived and designed the experiments; R.V., M.V., A.S., and S.P. performed the experiments and analyzed the data; R.V. and M.V. wrote the paper.

Funding

This research was funded by a Mercer University Seed Grant, Mercer Undergraduate Biomedical Scholar (MUBS) Program Award to S.P., and generous support from the Landings Women's Golf Association (LWGA).

Conflicts-of-interest disclosure

The authors declare no competing financial interests.

References

Allemand, J.F., Maier, B., Smith, D.E., 2012. Molecular motors for DNA translocation in prokaryotes. Curr. Opin. Biotechnol. 23, 503–509.
Baer, R., Bankier, A.T., Biggin, M.D., Deininger, P.L., Farrell, P.J., Gibson, T.J., Hatfull, G., Hudson, G.S., Satchwell, S.C., Seguin, C., et al., 1984. DNA sequence and expression of the B95-8 Epstein-Barr virus genome. Nature 310, 207–211.
Balfour Jr., H.H., Dunmire, S.K., Hogquist, K.A., 2015. Infectious mononucleosis. Clin. Transl. Immunol. 4, e33.
Berman, H.M., Westbrook, J., Feng, Z., Gilliland, G., Bhat, T.N., Weissig, H., Shindyalov, I.N., Bourne, P.E., 2000. The protein data bank. Nucleic Acids Res. 28, 235–242.
Cai, M., Liao, Z., Chen, T., Wang, P., Zou, X., Wang, Y., Xu, Z., Jiang, S., Huang, J., Chen, D., Peng, T., Hong, G., Li, M., 2017. Characterization of the subcellular localization of Epstein-Barr virus encoded proteins in live cells. Oncotarget 8, 70006–70034.
Chen, J., 2012. Roles of the PI3K/Akt pathway in Epstein-Barr virus-induced cancers and therapeutic implications. World J. Virol. 1, 154–161.
Cohen, J.I., Fauci, A.S., Varmus, H., Nabel, G.J., 2011. Epstein-Barr virus: an important vaccine target for cancer prevention. Sci. Transl. Med. 3 (107fs107).
Cui, X., Cao, Z., Chen, Q., Arjunaraja, S., Snow, A.L., Snapper, C.M., 2016. Rabbits immunized with Epstein-Barr virus gH/gL or gB recombinant proteins elicit higher serum virus neutralizing activity than gp350. Vaccine 34, 4050–4055.
Deng, B., O'Connor, C.M., Kedes, D.H., Zhou, Z.H., 2007. Direct visualization of the putative portal in the Kaposi's sarcoma-associated herpesvirus capsid by cryoelectron tomography. J. Virol. 81, 3640–3644.
Dittmer, A., Bogner, E., 2005. Analysis of the quaternary structure of the putative HCMV portal protein PUL104. Biochemistry 44, 759–765.
Dolcetti, R., Dal Col, J., Martorelli, D., Carbone, A., Klein, E., 2013. Interplay among viral antigens, cellular pathways and tumor microenvironment in the pathogenesis of EBV-driven lymphomas. Semin. Cancer Biol. 23, 441–456.
Eiz-Vesper, B., Maecker-Kolhoff, B., Blasczyk, R., 2012. Adoptive T-cell immunotherapy from third-party donors: characterization of donors and set up of a T-cell donor registry. Front. Immunol. 3, 410.
Feng, W.H., Hong, G., Delecluse, H.J., Kenney, S.C., 2004. Lytic induction therapy for Epstein-Barr virus-positive B-cell lymphomas. J. Virol. 78, 1893–1902.
George, L.C., Rowe, M., Fox, C.P., 2012. Epstein-barr virus and the pathogenesis of T and NK lymphoma: a mystery unsolved. Curr. Hematol. Malig. Rep. 7, 276–284.
Gershburg, E., Pagano, J.S., 2005. Epstein-Barr virus infections: prospects for treatment. J. Antimicrob. Chemother. 56, 277–281.
Giunco, S., Celeghin, A., Gianesin, K., Dolcetti, R., Indraccolo, S., De Rossi, A., 2015. Cross talk between EBV and telomerase: the role of TERT and NOTCH2 in the switch of latent/lytic cycle of the virus. Cell Death Dis. 6, e1774.
Holzenburg, A., Dittmer, A., Bogner, E., 2009. Assembly of monomeric human cytomegalovirus pUL104 into portal structures. J. Gen. Virol. 90, 2381–2385.
Hong, G.K., Gulley, M.L., Feng, W.H., Delecluse, H.J., Holley-Guthrie, E., Kenney, S.C., 2005. Epstein-Barr virus lytic infection contributes to lymphoproliferative disease in a SCID mouse model. J. Virol. 79, 13993–14003.
Houldcroft, C.J., Kellam, P., 2015. Host genetics of Epstein-Barr virus infection, latency and disease. Rev. Med. Virol. 25, 71–84.
Howard, A.J., Sherman, D.M., Visalli, M.A., Burnside, D.M., Visalli, R.J., 2012. The Varicella-zoster virus ORF54 gene product encodes the capsid portal protein, pORF54. Virus Res. 167, 102–105.
Hu, L., Lin, Z., Wu, Y., Dong, J., Zhao, B., Cheng, Y., Huang, P., Xu, L., Xia, T., Xiong, D., Wang, H., Li, M., Guo, L., Kieff, E., Zeng, Y., Zhong, Q., Zeng, M., 2016. Comprehensive profiling of EBV gene expression in nasopharyngeal carcinoma through paired-end transcriptome sequencing. Front. Med. 10, 61–75.
Hui, K.F., Tam, K.P., Chiang, A.K.S., 2017. Therapeutic strategies against epstein-barr virus-associated cancers using proteasome inhibitors. Viruses 9.
Jha, H.C., Banerjee, S., Robertson, E.S., 2016. The role of gammaherpesviruses in cancer pathogenesis. Pathogens 5.
Kanakry, J.A., Ambinder, R.F., 2013. EBV-related lymphomas: new approaches to treatment. Curr. Treat. Options Oncol. 14, 224–236.
Klein, E., Kis, L.L., Klein, G., 2007. Epstein-Barr virus infection in humans: from harmless to life endangering virus-lymphocyte interactions. Oncogene 26, 1297–1305.
Kornfeind, E.M., Visalli, R.J., 2018. Human herpesvirus portal proteins: structure, function, and antiviral prospects. Rev. Med. Virol. 28, e1972.
Kosowicz, J.G., Lee, J., Peiffer, B., Guo, Z., Chen, J., Liao, G., Hayward, S.D., Liu, J.O., Ambinder, R.F., 2017. Drug modulators of B cell signaling pathways and epstein-barr virus lytic activation. J. Virol. 91.
Lee, H.G., Kim, H., Kim, E.J., Park, P.G., Dong, S.M., Choi, T.H., Kim, H., Chong, C.R., Liu, J.O., Chen, J., Ambinder, R.F., Hayward, S.D., Park, J.H., Lee, J.M., 2015. Targeted therapy for Epstein-Barr virus-associated gastric carcinoma using low-dose gemcitabine-induced lytic activation. Oncotarget 6, 31018–31029.
Li, H., Liu, S., Hu, J., Luo, X., Li, N., A, M.B., Cao, Y., 2016. Epstein-Barr virus lytic reactivation regulation and its pathogenic role in carcinogenesis. Int. J. Biol. Sci. 12, 1309–1318.
Lin, M.C., Lin, Y.C., Chen, S.T., Young, T.H., Lou, P.J., 2017. Therapeutic vaccine targeting Epstein-Barr virus latent protein, LMP1, suppresses LMP1-expressing tumor growth and metastasis in vivo. BMC Cancer 17, 18.
Lorenzen, K., Olia, A.S., Uetrecht, C., Cingolani, G., Heck, A.J., 2008. Determination of stoichiometry and conformational changes in the first step of the P22 tail assembly. J. Mol. Biol. 379, 385–396.
Lurz, R., Orlova, E.V., Gunther, D., Dube, P., Droge, A., Weise, F., van Heel, M., Tavares, P., 2001. Structural organisation of the head-to-tail interface of a bacterial virus. J. Mol. Biol. 310, 1027–1037.
Ma, S.D., Hegde, S., Young, K.H., Sullivan, R., Rajesh, D., Zhou, Y., Jankowska-Gan, E.,

Burlingham, W.J., Sun, X., Gulley, M.L., Tang, W., Gumperz, J.E., Kenney, S.C., 2011. A new model of Epstein-Barr virus infection reveals an important role for early lytic viral protein expression in the development of lymphomas. J. Virol. 85, 165–177.
McElwee, M., Vijayakrishnan, S., Rixon, F., Bhella, D., 2018. Structure of the herpes simplex virus portal-vertex. PLoS Biol. 16, e2006191.
McLaughlin, L.P., Bollard, C.M., Keller, M.D., 2018. Adoptive T cell therapy for epstein-barr virus complications in patients with primary immunodeficiency disorders. Front. Immunol. 9, 556.
Mettenleiter, T.C., Klupp, B.G., Granzow, H., 2006. Herpesvirus assembly: a tale of two membranes. Curr. Opin. Microbiol. 9, 423–429.
Motwani, T., Lokareddy, R.K., Dunbar, C.A., Cortines, J.R., Jarrold, M.F., Cingolani, G., Teschke, C.M., 2017. A viral scaffolding protein triggers portal ring oligomerization and incorporation during procapsid assembly. Sci. Adv. 3, e1700423.
Münz, C., 2015. **Preface**. Curr. Top. Microbiol. Immunol. 390(Pt 1), v–vi.
Newcomb, W.W., Juhas, R.M., Thomsen, D.R., Homa, F.L., Burch, A.D., Weller, S.K., Brown, J.C., 2001. The UL6 gene product forms the portal for entry of DNA into the herpes simplex virus capsid. J. Virol. 75, 10923–10932.
Oliveira, L., Tavares, P., Alonso, J.C., 2013. Headful DNA packaging: bacteriophage SPP1 as a model system. Virus Res. 173, 247–259.
Pavlova, S., Feederle, R., Gartner, K., Fuchs, W., Granzow, H., Delecluse, H.J., 2013. An Epstein-Barr virus mutant produces immunogenic defective particles devoid of viral DNA. J. Virol. 87, 2011–2022.
Rajcani, J., Szenthe, K., Banati, F., Szathmary, S., 2014. Survey of Epstein Barr virus (EBV) immunogenic proteins and their epitopes: implications for vaccine preparation. Recent Pat. anti-Infect. Drug Discov. 9, 62–76.
Russo, J.J., Bohenzky, R.A., Chien, M.C., Chen, J., Yan, M., Maddalena, D., Parry, J.P., Peruzzi, D., Edelman, I.S., Chang, Y., Moore, P.S., 1996. Nucleotide sequence of the Kaposi sarcoma-associated herpesvirus (HHV8). Proc. Natl. Acad. Sci. USA 93, 14862–14867.
Stoker, S.D., Novalic, Z., Wildeman, M.A., Huitema, A.D., Verkuijlen, S.A., Juwana, H., Greijer, A.E., Tan, I.B., Middeldorp, J.M., de Boer, J.P., 2015. Epstein-Barr virus-targeted therapy in nasopharyngeal carcinoma. J. Cancer Res. Clin. Oncol. 141, 1845–1857.
Topalis, D., Gillemot, S., Snoeck, R., Andrei, G., 2018. Thymidine kinase and protein kinase in drug-resistant herpesviruses: heads of a Lernaean Hydra. Drug Resist. Updates : Rev. Comment. Antimicrob. Anticancer Chemother. 37, 1–16.
Tse, E., Kwong, Y.L., 2015. Epstein Barr virus-associated lymphoproliferative diseases: the virus as a therapeutic target. Exp. Mol. Med. 47, e136.
Turner, J.E., Taylor, G.S., 2013. Epstein–Barr virus: opportunities for prophylactic and therapeutic vaccines. Micorbiol. Today.
van Zeijl, M., Fairhurst, J., Jones, T.R., Vernon, S.K., Morin, J., LaRocque, J., Feld, B., O'Hara, B., Bloom, J.D., Johann, S.V., 2000. Novel class of thiourea compounds that inhibit herpes simplex virus type 1 DNA cleavage and encapsidation: resistance maps to the UL6 gene. J. Virol. 74, 9054–9061.
Visalli, R.J., Fairhurst, J., Srinivas, S., Hu, W., Feld, B., DiGrandi, M., Curran, K., Ross, A., Bloom, J.D., van Zeijl, M., Jones, T.R., O'Connell, J., Cohen, J.I., 2003. Identification of small molecule compounds that selectively inhibit varicella-zoster virus replication. J. Virol. 77, 2349–2358.
Visalli, R.J., Howard, A.J., 2014. Non-axial view of the varicella-zoster virus portal protein reveals conserved crown, wing and clip architecture. Intervirology 57, 121–125.
Visalli, R.J., van Zeijl, M., 2003. DNA encapsidation as a target for anti-herpesvirus drug therapy. Antivir. Res. 59, 73–87.
Walling, D.M., Flaitz, C.M., Nichols, C.M., 2003. Epstein-Barr virus replication in oral hairy leukoplakia: response, persistence, and resistance to treatment with valacyclovir. J. Infect. Dis. 188, 883–890.
White, C.A., Stow, N.D., Patel, A.H., Hughes, M., Preston, V.G., 2003. Herpes simplex virus type 1 portal protein UL6 interacts with the putative terminase subunits UL15 and UL28. J. Virol. 77, 6351–6358.
Wildeman, M.A., Novalic, Z., Verkuijlen, S.A., Juwana, H., Huitema, A.D., Tan, I.B., Middeldorp, J.M., de Boer, J.P., Greijer, A.E., 2012. Cytolytic virus activation therapy for Epstein-Barr virus-driven tumors. Clin. Cancer Res. 18, 5061–5070.
Yang, J., Yan, R., Roy, A., Xu, D., Poisson, J., Zhang, Y., 2015. The I-TASSER Suite: protein structure and function prediction. Nat. Methods 12, 7–8.
Yang, K., Baines, J.D., 2008. Domain within herpes simplex virus 1 scaffold proteins required for interaction with portal protein in infected cells and incorporation of the portal vertex into capsids. J. Virol. 82, 5021–5030.
Yasui, R., Yoshida, C., Yamaguchi, T., Inoue, N., 2017. Characterization of an anti-varicella-zoster virus compound that targets the portal protein encoded by ORF54. Microbiol. Immunol. 61, 398–402.
Yu, F., Lu, Y., Petersson, F., Wang, D.Y., Loh, K.S., 2018. Presence of lytic Epstein-Barr virus infection in nasopharyngeal carcinoma. Head Neck 40, 1515–1523.